Check for updates

AGU ADVANCING EARTH AND SPACE SCIENCE

Geophysical Research Letters

RESEARCH LETTER
10.1029/2023GL103042

Extreme Flood Sediment Production and Export Controlled by Reach-Scale Morphology

E. R. C. Baynes[1], M. E. Kincey[2], and J. Warburton[3]

[1]Geography and Environment, Loughborough University, Loughborough, UK, [2]School of Geography, Politics and Sociology, Newcastle University, Newcastle upon Tyne, UK, [3]Department of Geography, Durham University, Durham, UK

Key Points:

- Impact of extreme flood events on individual catchments differs according to their morphology
- Channel steepness is the first order control on volume of sediment production
- Sharp morphological transitions between river reaches promote enhanced sediment production and mobilization

Supporting Information:

Supporting Information may be found in the online version of this article.

Correspondence to:

E. R. C. Baynes,
e.baynes@lboro.ac.uk

Citation:

Baynes, E. R. C., Kincey, M. E., & Warburton, J. (2023). Extreme flood sediment production and export controlled by reach-scale morphology. *Geophysical Research Letters*, *50*, e2023GL103042. https://doi.org/10.1029/2023GL103042

Received 27 JAN 2023
Accepted 11 MAY 2023

Author Contributions:

Conceptualization: E. R. C. Baynes, M. E. Kincey, J. Warburton
Data curation: E. R. C. Baynes, M. E. Kincey, J. Warburton
Formal analysis: E. R. C. Baynes, M. E. Kincey, J. Warburton
Funding acquisition: E. R. C. Baynes, M. E. Kincey, J. Warburton
Investigation: E. R. C. Baynes, M. E. Kincey, J. Warburton
Methodology: E. R. C. Baynes, M. E. Kincey, J. Warburton
Project Administration: E. R. C. Baynes, M. E. Kincey, J. Warburton
Resources: E. R. C. Baynes, M. E. Kincey, J. Warburton

© 2023. The Authors.
This is an open access article under the terms of the Creative Commons Attribution-NonCommercial-NoDerivs License, which permits use and distribution in any medium, provided the original work is properly cited, the use is non-commercial and no modifications or adaptations are made.

Abstract Rapid earth surface evolution is discrete in nature, with short-duration extreme events having a widespread impact on landscapes despite occurring relatively infrequently. Here, we exploit a unique opportunity to identify the broad, process-based, controls on sediment production and export during extreme rainfall-runoff events through a multi-catchment analysis. A 3 hr extreme rainfall event generated significantly different impacts across three catchments, ranging from (a) sediment export exceeding two orders of magnitude more than the typical long term average to (b) a minimal impact, with this variability primarily controlled by catchment steepness and the presence of reach-scale morphological transitions caused by postglacial landscape adjustment. In any catchment worldwide where populations are at risk, we highlight the importance of combining topographic analysis with detailed mapping of channel bed material (e.g., presence of transitions between process domains) and identification of sediment sources within morphological transition zones for accurately predicting the impact of extreme events.

Plain Language Summary Extreme events, such as floods, can cause significant damage to landscapes leading to widespread erosion and deposition of sediment. Here, we identify the critical controls on sediment export from river catchments by examining the changes caused by a single high magnitude flood event on three contrasting river catchments. We show that local, reach-scale, variability in the river network is critical for determining the patterns of sediment erosion, with conditions in one of our study catchments allowing the flood to generate the equivalent of ~100 times the typical annual erosion in a very short period of time. Our results are important for allowing the identification of catchments potentially at risk of experiencing dramatic changes during extreme events in the future, due to their catchment characteristics.

1. Introduction

Rapid earth surface evolution is discrete in nature, with long periods of quiescence punctuated by relatively short-duration events when the majority of geomorphic work takes place (Baynes et al., 2015; Jones et al., 2021). In extreme cases, infrequent high-magnitude events can leave a long-lasting legacy on the landscape and dominate long-term evolution by contributing to widespread erosion, sediment production, transport and deposition within catchments (Benda & Dunne, 1997; Duller et al., 2014). Such events are typically characterized by very high river runoff, large volumes of sediment production and transport, leading to rapid landscape change and potentially hazardous conditions for local communities (Cook et al., 2018). Following rare extreme events, landscapes enter a period of recovery during which they gradually return to background conditions and sediment export rates (Brunsden & Thornes, 1979; Hovius et al., 2011; Marc et al., 2015). The balance between the recovery timescale and the magnitude and frequency of extreme events determines whether a landscape is in a transient state (e.g., continually eroding or aggrading) over the long-term (Allen, 2008; Duller et al., 2014). Despite this, our understanding of the fundamental mechanisms that control the impact of extreme events on landscapes remains limited, as it is based on observations of the local morphological impact of extreme events that typically occur within single catchments (e.g., Licciardello et al., 2019; Milan, 2012; Scorpio et al., 2022). Therefore, it is difficult to develop a broadly-applicable predictive tool that can establish the expected future impact of extreme events in diverse catchments. Over-reliance on identifying the impacts of extreme events from single catchments means subtle controls of catchment morphology could be overlooked. With the frequency and magnitude of rainfall-induced extreme events expected to increase in the future as a result of climate changes (Madsen et al., 2014), it is therefore critical to increase the quantitative understanding of the key controls that govern the impact of extreme events on landscapes.

Software: E. R. C. Baynes, M. E. Kincey, J. Warburton
Validation: E. R. C. Baynes, M. E. Kincey, J. Warburton
Visualization: E. R. C. Baynes, M. E. Kincey, J. Warburton
Writing – original draft: E. R. C. Baynes
Writing – review & editing: E. R. C. Baynes, M. E. Kincey, J. Warburton

Devrani et al. (2015) identified that the steepness of river long profiles relative to their upstream catchment area is a useful first-order indicator for the magnitude of geomorphic change during extreme flood events. However, it has also been shown that morphological diversity within catchments, such as lithological boundaries or channel geometry variability, can be important at controlling local patterns of sediment production and transport (Beer et al., 2016; Chartrand et al., 2018; Czuba & Foufoula-Georgiou, 2015; Fryirs et al., 2007; Venditti et al., 2014). Here, we exploit a unique opportunity to identify the critical landscape features, beyond first order channel steepness, that control the production, mobilization, and export of sediment from steep upland catchments during extreme flood events. By quantifying sediment production and export from three closely situated, but contrasting, upland catchments that were all impacted by the same extreme rainfall-runoff event in 2019 (Figure 1), we can highlight the critical landscape features that characterize areas at high risk of significant landscape change and associated geohazards related to extreme events, that are expected to become more frequent in the future (Archer & Fowler, 2021; Madsen et al., 2014).

2. Study Area: Upper River Swale Catchment and the 2019 Extreme Rainfall-Runoff Event

On 30 July 2019, an area of low air pressure and thunderstorms impacted northern England, with rainfall intensities peaking at >60 mm per hour between 1400 and 1700 GMT (Sefton et al., 2021). The extreme rainfall-runoff event was focused on the steep upland, glacially-modified, catchment of the Upper River Swale and the primary sub-catchment of Arkle Beck (Figure 1), causing widespread impacts to the river channels, infrastructure, properties, and industrial heritage sites including abandoned metal mine sites (Dennis et al., 2009; Macklin et al., 1997). First order tributaries to the River Swale and Arkle Beck include Slei Gill, Grinton Beck, and Barney Beck which are connected directly to the trunk channels but have distinct catchment morphologies in terms of shape, steepness, and postglacial adjustment despite relatively similar drainage areas and stream lengths (Figure 1). Slei Gill, for example, is approximately square in shape (Catchment Area = 4.27 km^2; Stream Length = 3,760 m; Basin relief = 283 m; Relief Ratio = 0.075; Elongation Ratio = 0.62; Mean normalized channel steepness, K_{Sn}, = 50.9; Table S1 in Supporting Information S1) and has a steep, incised, bedrock-lined reach mid-catchment, whereas Grinton Beck is smaller, more elongate (Catchment Area = 1.33 km^2; Stream Length = 3,390 m; Basin relief = 283 m; Relief Ratio = 0.067; Elongation Ratio = 0.38; Mean K_{Sn} = 27.9; Table S1 in Supporting Information S1), and has a steep, incised, reach near the tributary outlet (Figure 1). Barney Beck is the largest and longest catchment, but has a similar basin relief to the others (Catchment Area = 5.60 km^2; Stream Length = 6,170 m; Basin relief = 268 m; Relief Ratio = 0.044; Elongation Ratio = 0.43; Mean K_{Sn} = 27.3; Table S1 in Supporting Information S1). Quantifying the impact of the extreme rainfall event in 2019 in morphologically distinct tributaries less than 5 km apart provides a unique opportunity to go beyond a local assessment of the extreme flood impacts in a single catchment. In this study, we identify the critical features that control the magnitude and pattern of sediment production, mobilization, and export, and ultimately the vulnerability of catchments to significant morphological change, and downstream sediment flux, during extreme events.

Analysis of archival records in the study area, collated by Archer and Fowler (2021), referencing terms such as "cloudburst" or "severe thunderstorm" that caused severe damage to infrastructure comparable with 2019 (e.g., bridges washed away), indicate that eight similar events occurred in 318 years (in 1701, 1771, 1822, 1864, 1883, 1888, and 1914). Such destructive landscape-defining events therefore have an average occurrence of one event per ~40 years. Although the exact hydrological definition and precise morphological impacts of these historic floods are unknown, it is clear from documented accounts these discrete events dominate the long term sediment production and transfer from the headwater tributaries. The decades between the discrete high magnitude events are "recovery" periods of quiescence (Allen, 2008; Brunsden & Thornes, 1979).

3. Data and Methods

The assessment of the morphological impact of the July 2019 extreme rainfall-runoff event on Slei Gill, Grinton Beck, and Barney Beck was carried out by detailed field surveys and the comparison of high resolution topography collected pre- and post-event. For the pre-event topography, we used 1 m spatial resolution lidar data collected in 2016 from the Environment Agency National Lidar Programme which is freely available under the Open Government License (Environment Agency, 2022). For post-event topography, we used centimeter-resolution point clouds created using Structure-from-Motion (e.g., Westoby et al., 2012) from aerial UAV surveys commissioned by the Environment Agency in March 2021 (Section S2 and Tables S2–S5 in Supporting Information S1). We

19448007, 2023, 10, Downloaded from https://agupubs.onlinelibrary.wiley.com/doi/10.1029/2023GL103042 by Test, Wiley Online Library on [02/11/2023]. See the Terms and Conditions (https://onlinelibrary.wiley.com/terms-and-conditions) on Wiley Online Library for rules of use; OA articles are governed by the applicable Creative Commons License

10.1029/2023GL103042

19448007, 2023, 10, Downloaded from https://agupubs.onlinelibrary.wiley.com/doi/10.1029/2023GL103042 by Test, Wiley Online Library on [02/11/2023]. See the Terms and Conditions (https://onlinelibrary.wiley.com/terms-and-conditions) on Wiley Online Library for rules of use; OA articles are governed by the applicable Creative Commons License

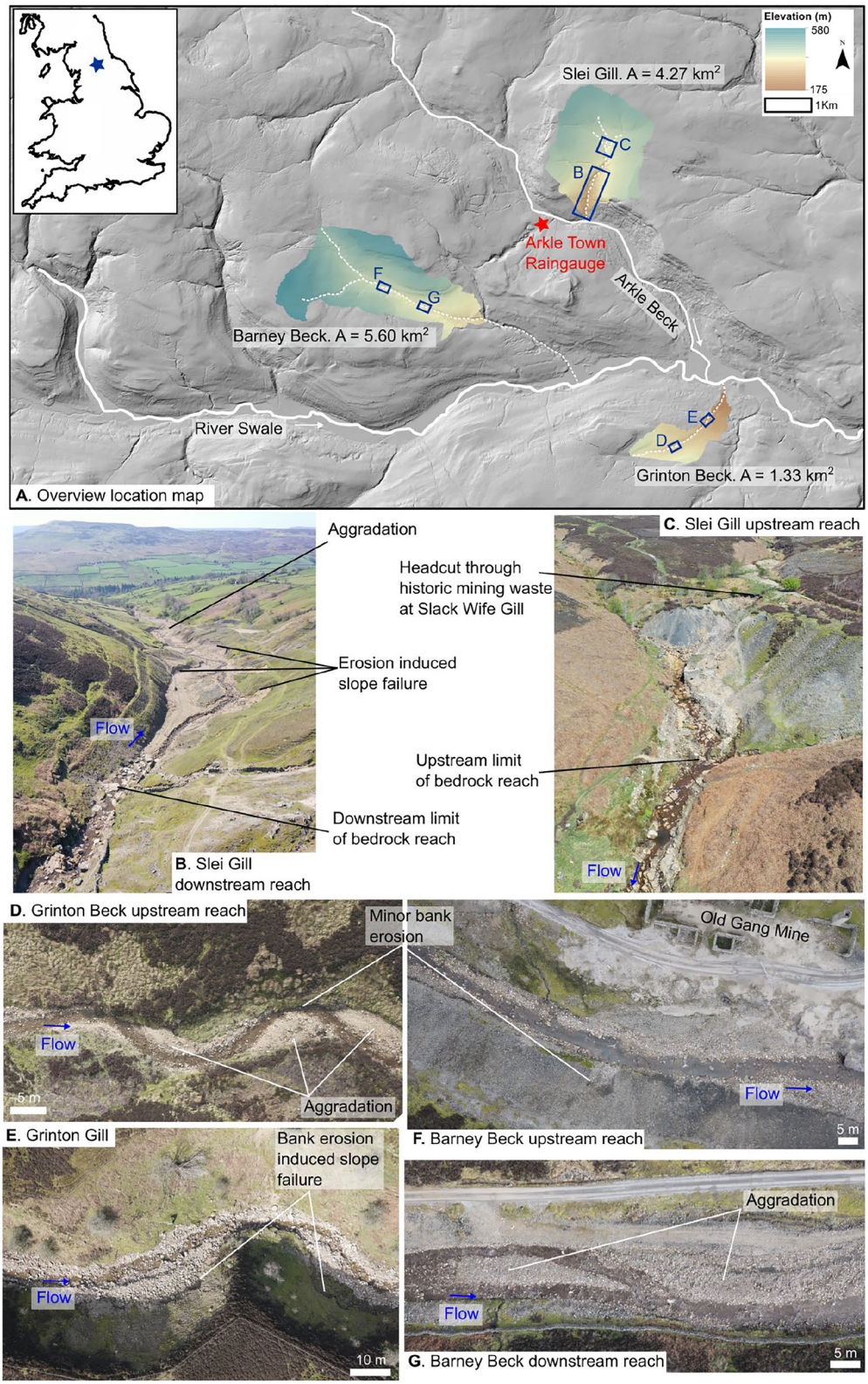

Figure 1. Overview location map (a) of the Upper River Swale, UK. The three study catchments are indicated by the colored elevation maps. Red star indicates Arkle Town raingauge. Panels (b–g) are post-flood aerial images of each catchment, with key morphological impacts highlighted (blue squares on overview map show location of aerial images). Note: panels (b–c) are oblique images (no scale bar) whereas (d–g) are vertical images.

19448007, 2023, 10, Downloaded from https://agupubs.onlinelibrary.wiley.com/doi/10.1029/2023GL103042 by Test, Wiley Online Library on [02/11/2023]. See the Terms and Conditions (https://onlinelibrary.wiley.com/terms-and-conditions) on Wiley Online Library for rules of use; OA articles are governed by the applicable Creative Commons License

performed an additional UAV survey in April 2022 to extend the spatial extent of the post-event topography data to cover the upper reaches of Slei Gill that were missed in the 2021 survey but where field observations indicated significant morphological change (e.g., headcut at Slack Wife Gill; Figure 1c). While the post-event topographic surveys were not collected immediately after the event in 2019, no similar extreme rainfall-runoff events occurred between 2019 and 2022 and regular field visits indicated no significant surface changes such that we can be confident the measured difference in topography in the pre-and post-event data sets are the result of the 2019 flood. Vertical differences in elevation between pre and post-flood topography were calculated directly on the point clouds using the M3C2 algorithm (Lague et al., 2013) in CloudCompare (CloudCompare, 2022; Figures S1–S3 in Supporting Information S1) and exported as rasters for further analysis. The maps of elevation change were ground-truthed during field visits and through analysis of post-flood aerial imagery (e.g., Figures 1b–1g).

We used the three-hour event rainfall record from the Arkle Town raingauge (Met Office, 2019), located 1 km from Slei Gill, 2.5 km from Barney Beck and 5 km from Grinton Beck (Figure 1a), and the pre-flood topography as input data for the HEC-RAS 2D hydrodynamic model version 2.6.1. In the absence of flow gauging data within each catchment, we used the direct precipitation "rain-on-grid" option within HEC-RAS to simulate the flooded extent within each catchment. The HEC-RAS outputs (Figures S4–S6 in Supporting Information S1) provide useful estimates of the spatial coverage of the maximum wetted area and water depth in the channels during the extreme rainfall-runoff event (Costalile et al., 2021), and were verified as matching the flood extent from field observations.

Topographic analysis was performed on the topography (lidar DEM), elevation change (M3C2), and flood water depth (HEC-RAS) rasters using the Topotoolbox algorithms in Matlab (Schwanghart & Scherler, 2014). We extracted the location of the stream networks of the three tributaries and calculated the normalized channel steepness (K_{sn}; Flint, 1974) of the river long profiles from each DEM. We used a mask of the channel location during the flood (from the HEC-RAS output) to calculate the within channel elevation change, and set a 30 m buffer around the channel location mask to calculate the elevation changes on the directly coupled, unvegetated, hillslopes. The 30 m buffer for the hillslopes covers all areas where significant topographic changes occurred within the catchments (Figures S1–S3 in Supporting Information S1). We also used the swath mapping tool within Topotoolbox, using the stream network as the center line of the swaths, to extract the following longitudinal information from the topographic data: (a) valley relief, calculated as elevation above the channel, (b) channel slope, and (c) channel width. We used the elevation change data within the channel and hillslope areas to calculate (a) the total volume of sediment produced within each catchment during the 2019 flood, (b) the volume of sediment exported from the catchment during the flood (Figures 2a–2d) and (c) the probability density function of elevation changes (Figure 2e) as a measure of the magnitude of changes within the catchments.

Using the slope and width data, we calculated the along-stream sediment transport capacity (Q_t) during the flood event (Croissant et al., 2017):

$$Q_t = WK\left(\rho_w g\left(\frac{nQ}{W}\right)^{0.6} S^{0.7} - (\rho_s - \rho_w) g \tau_c^* D_{50}\right)^{1.5} \quad (1)$$

where W is the channel width, K is a constant, ρ_w and ρ_s are the densities of water (1,000 kg m^{-3}) and sediment (2,800 kg m^{-3}) respectively, g is the acceleration due to gravity (9.81 m s^{-2}), n is the Manning"s roughness coefficient (0.06), Q is water discharge, S is the channel slope, τ_c^* is the critical shield"s stress (0.04) and D_{50} is the median sediment grain size. The longitudinal variation in Q was calculated from the HEC-RAS model output by summing the multiple of the water depth output, the water velocity output and the pixel size in a swath from the channel center line. To examine the spatial variability of Q_t within each catchment, we used the same values for D_{50} (0.05 m) and n (0.06) for all calculations and then calculated a normalized Q_t with distance downstream as the ratio of local Q_t to max Q_t. The quantified elevation changes combined with topographic analysis and field observations of catchment morphologies allow the identification of the key features that control the production, mobilization and export of sediment during extreme floods.

4. Morphological Impact of 2019 Flood

4.1. Sediment Production and Mobilization

The magnitude and source area of sediment mobilized during the 2019 rainfall-runoff event differed markedly between the three headwater catchments. The Slei Gill channel system received 18,770 m^3 from the adjoining

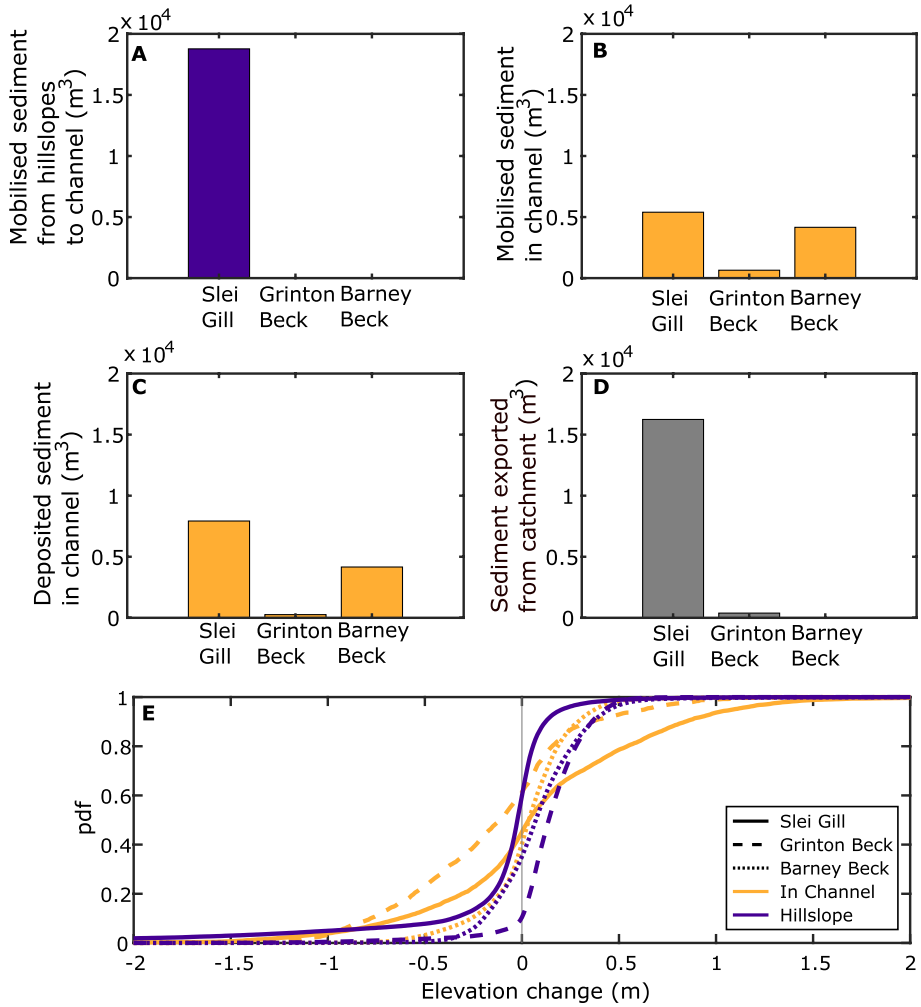

Figure 2. Summary of the morphological impact of the 2019 extreme flood event in Upper Swaledale, calculated using the pre- and post-flood topography. (a) Total volume of mobilized sediment from hillslopes to channel. (b) Total volume of mobilized sediment from in-channel locations. (c) Total sediment volume of stored in channel. (d) Total volume of sediment exported from the catchment, calculated as the sum of (a–c). (e) The probability density function of surface elevation change between pre- and post-flood topography for each catchment; hillslopes in purple and in-channel locations in orange. Gray line indicates threshold between erosion (negative elevation change) to deposition (positive elevation change).

hillslopes, whereas the Grinton Beck and Barney Beck received no hillslope material (Figure 2a). Erosive areas within the Slei Gill channel mobilized 5,400 m^3 of sediment, which was higher than areas in Grinton beck (650 m^3) and Barney Beck (4,160 m^3; Figure 2b). Depositional areas within the channels stored 7,930, 260, and 4,160 m^3 in Slei Gill, Grinton Beck and Barney Beck respectively (Figure 2b). The net sediment yield at the catchment outlet, calculated as the sum of hillslope material production and net in-channel erosion/deposition was 16,200 m^3 for Slei Gill, 390 m^3 Grinton Beck and 0 m^3 for Barney Beck (Figure 2d) (Reid & Dune, 1996). Averaged over the entire catchment, the sediment yield of the 2019 event was 0.0038 $m^3\ m^{-2}$ for Slei Gill and 0.00029 $m^3\ m^{-2}$ for Grinton Beck.

The upper estimate of the typical background suspended sediment yield in UK upland catchments is 0.000019 $m^3\ m^{-2}$ (calculated from 50 t km^{-2}, assuming a sediment density of 2,600 kg m^{-3}; Holliday et al., 2008). Estimating the relative contribution of suspended sediment and bedload to the long term sediment yield is inherently difficult (see Turowski et al., 2010 for detailed discussion), but assuming a generous estimate of 50:50 gives a long term average sediment yield of ~0.000038 $m^3\ m^{-2}$. Therefore we can estimate, acknowledging the uncertainty associated with the calculation, that the 2019 flood in Slei Gill contributed ~100 times more sediment in just a few hours than over a typical year, whereas Grinton Beck contributed ~7.5 times more sediment.

19448007, 2023, 10, Downloaded from https://agupubs.onlinelibrary.wiley.com/doi/10.1029/2023GL103042 by Test, Wiley Online Library on [02/11/2023]. See the Terms and Conditions (https://onlinelibrary.wiley.com/terms-and-conditions) on Wiley Online Library for rules of use; OA articles are governed by the applicable Creative Commons License

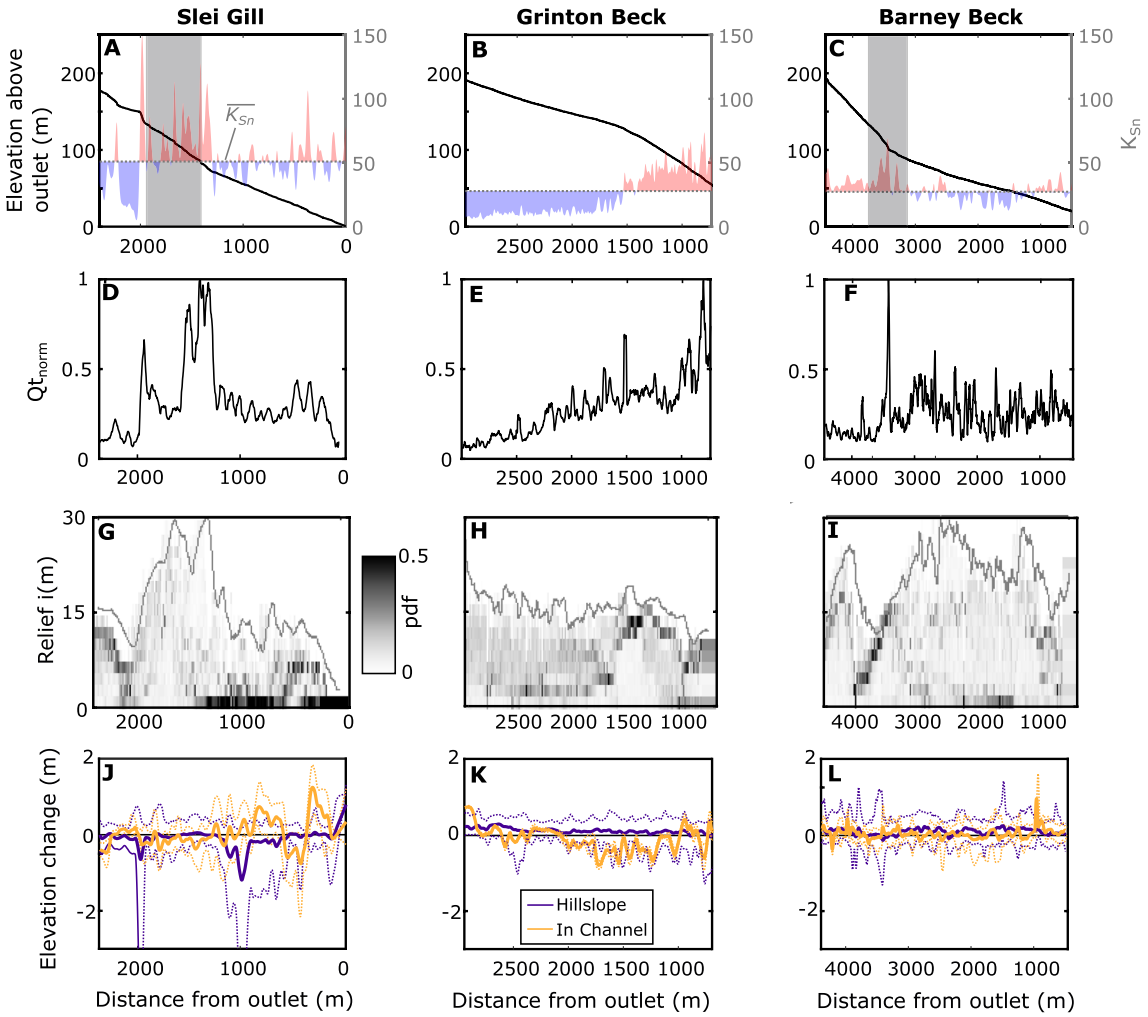

Figure 3. Spatial variability in morphological metrics that control the magnitude and location of erosion within each catchment during the 2019 flood. Left panels = Slei Gill. Middle panels = Grinton Beck. Right panels = Barney Beck. (a–c) River longitudinal profile in black, on left-axis. Right axis shows K_{sn}, plotted as anomalies from the mean value (horizontal gray line). Shaded red areas are reaches of the channel that are steeper than the mean K_{sn} for the catchment and shaded blue areas are reaches that are less steep than the mean K_{sn} for the catchment. Shaded gray areas indicate where the channel is confined by bedrock bed/banks. (d–f) Longitudinal variability in sediment transport capacity normalized according to the maximum sediment transport capacity for each catchment ($Q_{t,\mathrm{norm}}$). Plotted line is a 25 m moving average to aid visualization of the patterns within the data set. (g–i) Longitudinal variability in the probability density function (pdf) of valley relief within 150 m lateral swath of the channel centerline. Gray line indicates maximum valley relief within the swath at that location within the catchment. Darker shaded areas indicate higher density of locations within the swath at that elevation above the channel elevation. (j–l) Longitudinal variability in mean elevation change (solid lines) between pre- and post-flood topography in-channel (orange) and hillslopes (purple). Dashed lines indicate minimum and maximum values.

Figure 2e shows the pdf of elevation change in the channels and on the hillslopes within the catchments, with the majority of locations experiencing a relatively small magnitude of erosion or deposition. Importantly, Slei Gill has a large proportion of areas at higher negative elevation changes (<−1.5 m) on the hillslopes and also a large proportion of areas with higher positive changes (>0.5 m) in the channel, indicating aggradation whereas both Grinton Beck and Barney Beck have no locations that experienced such significant erosion (Figure 2f). This pattern matches field observations of major hillslope failures within Slei Gill that were not present in Grinton Beck and Barney Beck (Figures 1b–1g). In Slei Gill, some of that eroded hillslope material was deposited in the channel as shown by the large proportion of in-channel areas that experienced significant deposition (>0.5 m).

4.2. Spatial Controls on Flood Impact Magnitude

The shape of the river long profiles and channel steepness (K_{Sn}) varies between the three tributaries (Figures 3a–3c), with the mean K_{Sn} for Slei Gill higher (50.9) than Grinton Beck (27.8) and Barney Beck (27.3). Importantly, the

19448007, 2023, 10, Downloaded from https://agupubs.onlinelibrary.wiley.com/doi/10.1029/2023GL103042 by Test, Wiley Online Library on [02/11/2023]. See the Terms and Conditions (https://onlinelibrary.wiley.com/terms-and-conditions) on Wiley Online Library for rules of use; OA articles are governed by the applicable Creative Commons License

19448007, 2023, 10, Downloaded from https://agupubs.onlinelibrary.wiley.com/doi/10.1029/2023GL103042 by Test, Wiley Online Library on [02/11/2023]. See the Terms and Conditions (https://onlinelibrary.wiley.com/terms-and-conditions) on Wiley Online Library for rules of use; OA articles are governed by the applicable Creative Commons License

high positive K_{Sn} anomaly from the mean value (red areas in Figure 3a) highlights the very steep, bedrock lined, reach between 2000 and 1,300 m upstream from the outlet of Slei Gill (Figures 1b and 1c). Immediately downstream of the high positive K_{Sn} anomaly is a reach with a distinct negative K_{Sn} anomaly from the mean value (blue area in Figure 3a). Grinton Beck has two contrasting parts of the catchment with a steeper, incised, reach near the outlet (positive K_{Sn} anomaly) with the upper part of the catchment characterized by a lower slope and systematically negative K_{Sn} anomaly (Figure 3b). Superficially, Barney Beck has a similar long profile to Slei Gill with a steeper upper part before flatter reaches in the mid- to low- areas of the catchment, but both the mean K_{Sn} and the magnitude of the anomalies are relatively small in comparison to Slei Gill (Figure 3c).

As would be expected, the location of positive K_{Sn} anomalies match the pattern of along-stream sediment transport capacity (Q_t, which is highly dependent on slope; Equation 1; Figures 3d–3f) with the maximum Q_t values located in the reaches of highest K_{Sn}; in the upstream parts of Slei Gill and Barney Beck, and in the downstream part of Grinton Beck. The pattern of Q_t is also inversely related to pdf of valley relief (Figures 3g–3i) as a high density of relief pixels within the 150 m swath are close to 0 (e.g., Slei Gill from 0–1,200 m upstream and Barney Beck at 1,500–2,000 m upstream) indicating a wide flat valley floor (and low Q_t), whereas the high density of relief pixels above the channel indicate an incised valley with a narrow floor/channel width (e.g., Grinton Beck at 1,500 m upstream) that corresponds to high values of Q_t.

Figures 3j–3l shows the along-stream variation in elevation changes (i.e., erosion/deposition) on hillslopes and in-channel caused by the 2019 flood, with two clear zones within Slei Gill where significant hillslope erosion took place (at ∼2,000 m and ∼1,100 m upstream). These two zones locally coincide with the onset of a high K_{Sn} anomaly at 2,000 m upstream and the transition from a high to low K_{Sn} anomaly and a wide valley floor at 1,300 m (Figure 3j). Slei Gill experienced deposition in-channel downstream of the lower major hillslope failure between ∼1,000 and 800 m. The reach between 2000 and 1,300 m experienced small elevation changes during the flood despite high Q_t (Figure 3d) and high K_{Sn} (Figure 3a), because of the lack of sediment availability in this bedrock-lined reach. The low-slope reach with a wide valley floor close to the channel outlet (0–500 m upstream) experienced aggradation which is coincident with a reduction in Q_t at this location. In Grinton Beck (Figure 3k), the magnitude of erosion/aggradation was smaller than in Slei Gill, with erosion focused in-channel in the downstream reach at 1,500–1,000 m that coincides with a high K_{Sn} anomaly and high Q_t. In Barney Beck, the downstream reach from 3,000 to 1,500 m upstream (low K_{Sn} and Q_t) is characterized by aggradation with limited erosion throughout the channel (Figures 1f and 1g), supporting the overall pattern of sediment storage within the catchment rather than net sediment export (Figure 2).

5. Discussion

5.1. Importance of Extreme Events in Long Term Landscape Evolution

Using a sediment budget approach, we show that rare, extreme, events produce and mobilize substantially more sediment in just a few hours than over a typical year (∼100 times more in Slei Gill), highlighting the importance of such events for geomorphic work over the long term (Baynes et al., 2015; Jones et al., 2021). Given the resulting sediment availability within the channel from hillslope sources and relative frequency of similar events in the study region (∼ one per 40 years; Archer & Fowler, 2021), we hypothesize it is unlikely that Slei Gill will fully "recover" to typical UK upland sediment yields before the next perturbation event (Brunsden & Thornes, 1979), especially as extreme rainfall events are expected to become more frequent in the future (Madsen et al., 2014). We can therefore classify Slei Gill as being "transient" in nature (Allen, 2008; Duller et al., 2014) as a result of the July 2019 rainfall event, which further highlights the long-lasting legacy on landscape evolution of extreme events. Section 5.2 discusses the fundamental mechanisms that contribute to this long-term legacy, which are controlled by reach-scale morphological transitions.

5.2. The Role of Morphological Transitions in Producing and Exporting Sediment

Channel steepness is the first order control on the volume of sediment produced during extreme flood events (Figures 2 and 3a–3c), following Devrani et al. (2015). However, the detailed surveys, topographic analysis of along-stream variation in bed elevation change, topographic metrics and field observations of bed material (i.e., bedrock or alluvial) provide additional key information which demonstrates the importance of reach-scale morphological transitions for determining the production, mobilization, storage, and export of sediment during

19448007, 2023, 10, Downloaded from https://agupubs.onlinelibrary.wiley.com/doi/10.1029/2023GL103042 by Test, Wiley Online Library on [02/11/2023]. See the Terms and Conditions (https://onlinelibrary.wiley.com/terms-and-conditions) on Wiley Online Library for rules of use; OA articles are governed by the applicable Creative Commons License

extreme flood events. A sharp transition in the river long profile to high K_{Sn} generated a hotspot of significant erosion by the upstream migration of a headcut (Figures 1c, 3a, and 3j) through alluvial sediments in the upper part of Slei Gill. However, the second hotspot of significant erosion within Slei Gill occurred at the transition from high to low K_{Sn} (at 1,300 m) which is counterintuitive according to the first order slope control of Devrani et al. (2015). Here, we suggest that the significant erosion was caused by the emergence from the steep reach of high energy flow that was severely sediment-starved due to lack of sediment availability because of the bedrock-lined channel bed (Benda & Dunne, 1997). At the transition to the alluvial reach downstream of the bedrock-lined section, with the channel changing rapidly from detachment-limited to transport-limited conditions, the high energy flow, still with a relatively high Q_t, was able to erode and transport alluvial material from the bed and undermine adjoining hillslopes leading to their failure (Figure 1b) which created a hotspot of sediment production. Further downstream, there was aggradation due to the wider channel and low slope leading to the decline in Q_t (Czuba & Foufoula-Georgiou, 2015). We therefore highlight the critical role of transitions in bed material in addition to high K_{Sn} as very important controls on the spatial pattern of sediment mobilization and transport during extreme flood events. The locations of high K_{Sn} within a catchment are also important in determining the magnitude of sediment yield and whether the catchment is a net exporter of sediment during an extreme flood event. The primary sediment mobilization zone in Grinton Beck is directly connected to the catchment outlet as the incised channel reach of high K_{Sn} and high Q_t is located in the distal part of the catchment (Figures 1d, 1e, 3a, and 3e), whereas in Barney Beck the reach of high K_{Sn} is far removed (>3,000 m) from the outlet.

The reaches of high K_{Sn}, and their connectivity to the outlet, represent the efficiency of knickpoint headward propagation in the tributaries (Figures 3a and 3b) following the deglaciation of ice in the trunk channel ~12–15,000 years ago (Davies et al., 2019). The elevation of the valley floor in the trunk channel, due to overdeepening by ice, acts as a base level that the tributaries are adjusting to (Valla et al., 2010), and the zones of high K_{Sn} are the knickpoints that separate the downstream reaches that adjusted to the new base level from upstream reaches that are typically low relief with low slopes (e.g., Figure 3b). We therefore hypothesize that the extent of postglacial fluvial adjustment (i.e., headward knickpoint retreat and corresponding channel and hillslope adjustment; Baynes et al., 2022) is an important control on the morphological impact of extreme events. As demonstrated here, the zone of potential sediment mobilization is much larger and located higher up in the catchment in Slei Gill compared to Grinton Beck where sediment mobilization is focused in the downstream reach only. Catchments that are partially adjusted to new base level conditions which are often typical in headwater locations (Crosby & Whipple, 2006; Valla et al., 2010) are likely to have such morphological transitions (Baynes et al., 2022) and therefore incorporate more potential zones of high sediment mobilization compared to catchments with smooth concave river long profiles.

It is critical, therefore, to map and identify knickpoints, reach-scale morphological transitions within catchments, and their connectivity to the channel outlet in order to identify, mitigate, and manage the likely magnitude, and location, of sediment production during future extreme events within catchments. Detailed mapping of bedrock reaches, morphological transitions and storage buffer zones within catchments is required which can be performed in the field (e.g., Kincey et al., 2018) remotely from aerial imagery (e.g., Boothroyd et al., 2021; Carbonneau et al., 2004) or using topo-bathymetric lidar (e.g., Lague & Feldmann, 2020).

6. Conclusions

The impact of extreme flood events is controlled by the detailed morphological structure of the catchments, highlighted by the contrasting impact of the same extreme event on three adjacent tributaries of the Upper River Swale. Channel steepness is a first order control on the volume of sediment production and mobilization during extreme events, with the potential for significantly enhanced sediment mobilization when catchments contain sharp morphological transitions between reaches (e.g., from bedrock to alluvial). Using a multi-catchment approach, we show that the possible impact of future extreme flood events, could be better predicted using topographic analysis combined with detailed mapping of channel bed material and the careful identification of sediment sources within morphological transition zones.

Data Availability Statement

Pre-event topography data is openly sourced through the UK Environment Agency National Lidar Programme which is freely available under the Open Government License at https://www.data.gov.uk/dataset/f0db0249-f17b-4036-9e65-309148c97ce4/national-lidar-programme. The post-event topography surveys were collected as part

of the Water and Abandoned Metal Mines Programme, a partnership between the Environment Agency, the Coal Authority and the Department for Environment, Food and Rural Affairs. These data are available from the Zenodo repository: https://doi.org/10.5281/zenodo.7845255, alongside the processed DEMs of Difference and HEC-RAS output.

Acknowledgments
The research was funded by a grant from the Yorkshire Geological Society. We thank the landowners of the Grinton and East Arkengarthdale Estates for permission to conduct field work, Adam Bugg for his assistance in the field, and the Coal Authority and Environment Agency for sharing the March 2021 UAV survey data as part of the Water and Abandoned Metal Mines programme.

References

Allen, P. A. (2008). Time scales of tectonic landscapes and their sediment routing systems. In K. Gallagher, S. J. Jones, & J. Wainwright (Eds.), *Landscape evolution: Denudation, climate and tectonics over different time and space scales* (Vol. 296, pp. 7–28). Geological Society of London Special Publication.

Archer, D., & Fowler, H. (2021). A historical flash flood chronology for Britain. *Journal of Flood Risk Management*, *14*(3), e12721. https://doi.org/10.1111/jfr3.12721

Baynes, E. R. C., Attal, M., Niedermann, S., Kirstein, L. A., Dugmore, A. J., & Naylor, M. (2015). Erosion during extreme flood events dominates Holocene canyon evolution in northeast Iceland. *Proceedings of the National Academy of Sciences*, *112*(8), 2355–2360. https://doi.org/10.1073/pnas.1415443112

Baynes, E. R. C., Lague, D., Steer, P., & Davy, P. (2022). Dynamic bedrock channel width during knickpoint retreat enhances undercutting of coupled hillslopes. *Earth Surface Processes and Landforms*, *47*(15), 3629–3640. https://doi.org/10.1002/esp.5477

Beer, A. R., Turowski, J. M., & Kirchner, J. W. (2016). Spatial patterns of erosion in a bedrock gorge. *Journal of Geophysical Research: Earth Surface*, *122*(1), 191–214. https://doi.org/10.1002/2016jf003850

Benda, L., & Dunne, T. (1997). Stochastic forcing of sediment routing and storage in channel networks. *Water Resources Research*, *33*(12), 2865–2880. https://doi.org/10.1029/97wr02387

Boothroyd, R. J., Williams, R. D., Hoey, T. B., Barrett, B., & Prasajo, O. A. (2021). Applications of Google Earth Engine in fluvial geomorphology for detecting river channel change. *WIREs Water*, *8*(1), e21496. https://doi.org/10.1002/wat2.1496

Brunsden, D., & Thornes, J. B. (1979). Landscape sensitivity and change. *Transactions of the Institute of British Geographers*, *4*(4), 463–484. https://doi.org/10.2307/622210

Carbonneau, P. E., Lane, S. N., & Bergeron, N. E. (2004). Catchment-scale mapping of surface grain size in gravel bed rivers using airborne digital mapping. *Water Resources Research*, *40*, W07202. https://doi.org/10.1029/2003WR002759

Chartrand, S. M., Jellinek, A. M., Hassan, M. A., & Ferrer-Boix, C. (2018). Morphodynamics of a width-variable gravel bed stream: New insights on pool-Riffle formation from physical experiments. *Journal of Geophysical Research: Earth Surface*, *123*(11), 2735–2766. https://doi.org/10.1029/2017jf004533

CloudCompare. (2022). CloudCompare (version 2.11.3) (GPL software). Retrieved from http://www.cloudcompare.org

Cook, K. L., Andermann, C., Gimbert, F., Adhikari, B. R., & Hovius, N. (2018). Glacial lake outburst floods as drivers of fluvial erosion in the Himalaya. *Science*, *362*(6410), 53–57. https://doi.org/10.1126/science.aat4981

Costalile, P., Costanzo, C., Ferraro, D., & Barco, P. (2021). Is HEC-RAS 2D accurate enough for storm-event hazard assessment? Lessons learnt from a benchmarking study based on rain-on-grid modelling. *Journal of Hydrology*, *603*, 126962. https://doi.org/10.1016/j.jhydrol.2021.126962

Croissant, T., Lague, D., Steer, P., & Davy, P. (2017). Rapid post-seismic landslide evacuation boosted by dynamic river width. *Nature Geoscience*, *10*(9), 680–684. https://doi.org/10.1038/ngeo3005

Crosby, B. T., & Whipple, K. X. (2006). Knickpoint initiation and distribution within fluvial networks: 236 waterfalls in the Waipaoa River, North island, New Zealand. *Geomorphology*, *82*(1–2), 16–38. https://doi.org/10.1016/j.geomorph.2005.08.023

Czuba, J. A., & Foufoula-Georgiou, E. (2015). Dynamic connectivity in a fluvial network for identifying hotspots of geomorphic change. *Water Resources Research*, *51*(3), 1401–1421. https://doi.org/10.1002/2014wr016139

Davies, B. J., Livingstone, S. J., Roberts, D. H., Evans, D. J. A., Gheorghiu, D. M., & Cofaigh, C. (2019). Dynamic ice stream retreat in the central sector of the last British-Irish Ice Sheet. *Quaternary Science Reviews*, *225*, 105989. https://doi.org/10.1016/j.quascirev.2019.105989

Dennis, I. A., Coulthard, T. J., Brewer, P., & Macklin, M. G. (2009). The role of floodplains in attenuating contaminated sediment fluxes in formerly mined drainage basins. *Earth Surface Processes and Landforms*, *34*(3), 453–466. https://doi.org/10.1002/esp.1762

Devrani, R., Singh, V., Mudd, S. M., & Sinclair, H. D. (2015). Prediction of flash flood hazard impact from Himalayan river profiles. *Geophysical Research Letters*, *42*(14), 5888–5894. https://doi.org/10.1002/2015gl063784

Duller, R. A., Warner, N. H., McGonigle, C., De Angelis, S., Russell, A. J., & Mountney, N. P. (2014). Landscape reaction, response, and recovery following the catastrophic 1918 Katla jokulhlaup, southern Iceland. *Geophysical Research Letters*, *41*(12), 4214–4221. https://doi.org/10.1002/2014gl060090

Environment Agency. (2022). National LIDAR Programme online dataset. Retrieved from https://www.data.gov.uk/dataset/f0db0249-f17b-4036-9e65-309148c97ce4/national-lidar-programme

Flint, J. J. (1974). Stream gradient as a function of order, magnitude, and discharge. *Water Resources Research*, *10*(5), 969–973. https://doi.org/10.1029/wr010i005p00969

Fryirs, K. A., Brierley, G. J., Preston, N. J., & Kasai, M. (2007). Buffers, barriers and blankets: The (dis)connectivity of catchment-scale sediment cascades. *Catena*, *70*(1), 49–67. https://doi.org/10.1016/j.catena.2006.07.007

Holliday, V. J., Warburton, J., & Higgitt, D. L. (2008). Historic and contemporary sediment transfer in an upland Pennine catchment, UK. *Earth Surface Processes and Landforms*, *33*(14), 2139–2155. https://doi.org/10.1002/esp.1660

Hovius, N., Meunier, P., Lin, C.-W., Chen, H., Chen, Y.-G., Dadson, S., et al. (2011). Prolonged seismically induced erosion and the mass balance of a large earthquake. *Earth and Planetary Science Letters*, *304*(3–4), 347–355. https://doi.org/10.1016/j.epsl.2011.02.005

Jones, J. N., Boulton, S. J., Stokes, M., Bennett, G. L., & Whitworth, M. R. Z. (2021). 30-year record of Himalaya mass-easting reveals landscape perturbations by extreme events. *Nature Communications*, *12*(1), 6701. https://doi.org/10.1038/s41467-021-26964-8

Kincey, M. E., Warburton, J., & Brewer, P. (2018). Contaminated sediment flux from eroding abandoned historical metal mines: Spatial and temporal variability in geomorphological drivers. *Geomorphology*, *319*, 199–215. https://doi.org/10.1016/j.geomorph.2018.07.026

Lague, D., Brodu, N., & Leroux, J. (2013). Accurate 3D comparison of complex topography with terrestrial laser scanner: Application to the Rangitikei canyon (N-Z). *ISPRS Journal of Photogrammetry and Remote Sensing*, *82*, 10–26. https://doi.org/10.1016/j.isprsjprs.2013.04.009

Lague, D., & Feldmann, B. (2020). Topo-bathymetric airborne LiDAR for fluvial-geomorphology analysis. In *Developments in Earth surface processes* (Vol. 23, pp. 25–54).

Licciardello, F., Barbagallo, S., & Gallart, F. (2019). Hydrological and erosional response of a small catchment in Sicily. *Journal of Hydrology and Hydromechanics*, *67*(3), 201–212. https://doi.org/10.2478/johh-2019-0003

19448007, 2023, 10, Downloaded from https://agupubs.onlinelibrary.wiley.com/doi/10.1029/2023GL103042 by Test, Wiley Online Library on [02/11/2023]. See the Terms and Conditions (https://onlinelibrary.wiley.com/terms-and-conditions) on Wiley Online Library for rules of use; OA articles are governed by the applicable Creative Commons License

Macklin, M. G., Hudson-Edwards, K. A., & Dawson, E. J. (1997). The significance of pollution from historic metal mining in the Pennine orefields on river sediment contaminant fluxes to the North Sea. *Science of the Total Environment*, *194/195*, 391–397. https://doi.org/10.1016/s0048-9697(96)05378-8

Madsen, H., Lawrence, D., Lang, M., Martinkova, M., & Kjeldsen, T. R. (2014). Review of trend analysis and climate change projections of extreme precipitation and floods in Europe. *Journal of Hydrology*, *519*, 3634–3650. https://doi.org/10.1016/j.jhydrol.2014.11.003

Marc, O., Hovius, N., Uchida, T., & Hayashi, S. (2015). Transient changes of landslide rates after earthquakes. *Geology*, *42*(10), 883–886. https://doi.org/10.1130/g36961.1

Met Office. (2019). Heavy rainfall July 2019. Retrieved from https://www.metoffice.gov.uk/binaries/content/assets/metofficegovuk/pdf/weather/learn-about/uk-past-events/interesting/2019/2019_008_july_rainfall.pdf

Milan, D. (2012). Geomorphic impact and system recovery following an extreme flood in an upland stream: Thinhop Burn, northern England, UK. *Geomorphology*, *138*(1), 319–328. https://doi.org/10.1016/j.geomorph.2011.09.017

Reid, L. M., & Dune, T. (1996). Rapid evaluation of sediment budgets. In *Geo-ecology paperback* (p. 164). Catena Verlag GMBH.

Schwanghart, W., & Scherler, D. (2014). Topotoolbox 2 – MATLAB-based software for topographic analysis and modeling in Earth surface sciences. *Earth Surface Dynamics*, *2*, 1–7. https://doi.org/10.5194/esurf-2-1-2014

Scorpio, V., Cavalli, M., Steger, S., Crema, S., Marra, F., Zaramella, N., et al. (2022). Storm characteristics dictate sediment dynamics and geomorphic changes in mountain channels: A case study in the Italian Alps. *Geomorphology*, *402*, 108173. https://doi.org/10.1016/j.geomorph.2022.108173

Sefton, C., Muchan, K., Parry, S., Matthews, B., Barker, L. J., Turner, S., & Hannaford, J. (2021). The 2019/2020 floods in the UK: A hydrological appraisal. *Weather*, *76*(12), 378–384. https://doi.org/10.1002/wea.3993

Turowski, J. M., Rickenmann, D., & Dadson, S. J. (2010). The partitioning of the total sediment load of a river into suspended load and bedload: A review of empirical data. *Sedimentology*, *57*(4), 1126–1146. https://doi.org/10.1111/j.1365-3091.2009.01140.x

Valla, P. G., van der Beek, P. A., & Lague, D. (2010). Fluvial incision into bedrock: Insights from morphometric analysis and numerical modeling of gorges incising glacial hanging valleys (Western Alps, France). *Journal of Geophysical Research*, *115*, F02010. https://doi.org/10.1029/2008JF001079

Venditti, J. G., Rennie, C. D., Bomhof, J., Bradley, R. W., Little, M., & Church, M. (2014). Flow in bedrock canyons. *Nature*, *513*(7519), 435–537. https://doi.org/10.1038/nature13779

Westoby, M. J., Brasington, J., Glasser, N. F., Hambrey, M. J., & Reynolds, J. M. (2012). 'Structure-from-Motion' photogrammetry: A low-cost, effective tool for geoscience applications. *Geomorphology*, *179*, 300–314. https://doi.org/10.1016/j.geomorph.2012.08.021

19448007, 2023, 10, Downloaded from https://agupubs.onlinelibrary.wiley.com/doi/10.1029/2023GL103042 by Test, Wiley Online Library on [02/11/2023]. See the Terms and Conditions (https://onlinelibrary.wiley.com/terms-and-conditions) on Wiley Online Library for rules of use; OA articles are governed by the applicable Creative Commons License